

# Strong magneto-optical responses of an ensemble of defect-bound excitons in aged $WS_2$ and $WSe_2$ monolayers

Frederico B. Sousa,<sup>†</sup> Alessandra Ames,<sup>‡</sup> Mingzu Liu,<sup>¶,§</sup> Pedro L. Gastelois,<sup>||</sup>  
 Vinícius A. Oliveira,<sup>‡</sup> Da Zhou,<sup>¶,§</sup> Matheus J. S. Matos,<sup>⊥</sup> Helio Chacham,<sup>†</sup>  
 Mauricio Terrones,<sup>§,¶,#</sup> Marcio D. Teodoro,<sup>‡</sup> and Leandro M. Malard<sup>\*,†</sup>

<sup>†</sup>*Departamento de Física, Universidade Federal de Minas Gerais, Belo Horizonte, Minas Gerais 30123-970, Brazil*

<sup>‡</sup>*Departamento de Física, Universidade Federal de São Carlos, São Carlos, São Paulo 13565-905, Brazil*

<sup>¶</sup>*Department of Physics, The Pennsylvania State University, University Park, PA 16802, United States of America*

<sup>§</sup>*Center for 2-Dimensional and Layered Materials, The Pennsylvania State University, University Park, PA 16802, United States of America*

<sup>||</sup>*Centro de Desenvolvimento de Tecnologia Nuclear - CDTN, Belo Horizonte, Minas Gerais 31270-90, Brazil*

<sup>⊥</sup>*Departamento de Física, Universidade Federal de Ouro Preto, Ouro Preto, Minas Gerais 35400-000, Brazil*

<sup>#</sup>*Department of Materials Science and Engineering, The Pennsylvania State University, University Park, PA 16802, United States of America*

E-mail: lmalard@fisica.ufmg.br

## Abstract

Transition metal dichalcogenide (TMD) monolayers present a singular coupling in their spin and valley degrees of freedom. Moreover, by applying an external magnetic field it is possible to break the energy degeneracy between their K and  $-K$  valleys. Thus, this analogous valley Zeeman effect opens the possibility of controlling and distinguishing the spin and valley of charge carriers in TMDs by their optical transition energies, making these materials promising for the next generation of spintronic and photonic devices. However, the free excitons of pristine TMD monolayer samples present a moderate valley Zeeman splitting, which is measured by their g-factor values that are approximately  $-4$ . Therefore, for application purposes it is mandatory alternative excitonic states with higher magnetic responses. Here we investigate the valley Zeeman effect in aged  $\text{WS}_2$  and  $\text{WSe}_2$  grown monolayers by magneto-photoluminescence measurements at cryogenic temperatures. These samples present a lower energy defect-bound exciton emission related to defects adsorbed during the aging process. While the free excitons of these samples exhibit g-factors between  $-3$  and  $-4$ , their defect-bound excitons present giant effective g-factor values of  $-(25.0 \pm 0.2)$  and  $-(19.1 \pm 0.2)$  for  $\text{WS}_2$  and  $\text{WSe}_2$  aged monolayers, respectively. In addition, we observe a significant spin polarization of charge carriers in the defective mid gap states induced by the external magnetic fields. We explain this spin polarized population in terms of a spin-flip transition mechanism, which is also responsible for the magnetic dependent light emission of the defect-bound exciton states. Our work sheds light in the potential of aged TMDs as candidates for spintronic based devices.

## Introduction

Time reversal symmetry plays a major role in determining opposite spin states at the inequivalent K and  $-K$  valleys in monolayer TMDs.<sup>1</sup> Therefore, their valley selection rules lead to a coupling in the spin and valley degrees of freedom, allowing a selectively carrier excitation in both K and  $-K$  points by circular polarized light.<sup>2,3</sup> Moreover, by applying an

external magnetic field is possible to control the valence and conduction bands displacements due to an analogous Zeeman effect.<sup>4-7</sup> Since K and  $-K$  valleys present opposite spins, the band displacement is also contrary in each valley, resulting in an energy splitting of the K and  $-K$  excitons. Hence, the possibility of control the valley spin degree of freedom by an energy threshold makes the 2D TMDs promising for spin- and valleytronics.<sup>8</sup>

The valley Zeeman splitting has been investigated for optical transitions related to excitons,<sup>4-7,9,10</sup> trions,<sup>4-7,10,11</sup> biexcitons,<sup>10,12,13</sup> interlayer excitons,<sup>14-16</sup> Moiré excitons,<sup>17</sup> and defect-bound excitons<sup>18-24</sup> in distinct TMD monolayers and their heterostructures. This effect is usually measured by the optical transition g-factor, an unitless factor that relates the valley energy splitting with the magnetic field. Free exciton states in pristine TMD monolayers present a weak Zeeman energy shifting associated with g-factor values around  $-4$ , showing the necessity of engineering these materials to achieve stronger magnetic responses. In that sense, there are valley Zeeman splitting reports on defective TMDs that presented enhanced g-factors. For instance, vacancy-bound excitons in a MoS<sub>2</sub> monolayer showed a g-factor of  $-6.2$ ,<sup>23</sup> while defect-bound excitons related to single photon emitters in WSe<sub>2</sub> monolayers presented g-factors of approximately  $-10$ .<sup>18-21,24</sup> In addition, Fe- and Co-doped MoS<sub>2</sub> monolayers presented free exciton g-factors of  $-20$ <sup>25</sup> and  $-15$ ,<sup>26</sup> respectively, and a phase engineered WSe<sub>2</sub> monolayer displayed a free exciton g-factor of  $-14$ .<sup>27</sup>

Here we report an enhanced g-factor associated with an ensemble of defect-bound excitons in aged CVD grown WS<sub>2</sub> and WSe<sub>2</sub> monolayers by magneto-photoluminescence (PL) measurements with circularly polarized light detection, which was not shown in previous works. X-ray photoelectron spectroscopy (XPS) measurements revealed the presence of previously reported adsorbed defects in aged CVD grown monolayers, which are related to the emergence of multiple mid gap states. Power and temperature dependent PL experiments showed a lower energy peak associated with the defect-bound exciton state. Magneto-PL measurements with external magnetic fields from  $-9$  to  $9$  T unveiled g-factors of  $-(25.0 \pm 0.2)$  and  $-(19.1 \pm 0.2)$  for the lower energy PL peak in WS<sub>2</sub> and WSe<sub>2</sub> monolayers, respectively.

Besides, the defect-bound exciton emission displayed a significant degree of circular polarization induced by the external magnetic field, revealing a spin polarized charge carrier population in the mid gap states. This spin polarization leads to a magnetic field dependent distribution of charge carriers in the multiple mid gap states, which explains the great energy shift observed in the defect-bound exciton light emission. In addition, we propose a spin-flip transition mechanism to explain the magnetic field induced spin polarized population in the defective levels. Our work sheds light in the significant magnetic response of the defect-bound exciton emission related to aging defects in CVD grown WS<sub>2</sub> and WSe<sub>2</sub> monolayers, enlarging their applicability in spintronic devices.

## Results and discussion

To probe the presence of defects in an aged TMD sample and study the consequent modifications in its light emission, we performed power dependent PL measurements in a 2-year aged CVD grown WS<sub>2</sub> monolayer, as shown in Figures 1a,b. The power-dependent PL spectra of Figure 1a were taken at 4 K and are normalized by the free exciton ( $X_0$ ) peak ( $\sim 2.02$  eV), revealing a lower energy PL peak with a distinct intensity and energy position features. While the exciton PL peak presents no relevant shift in its energy and a linear intensity enhancement with respect to the incident power, the lower energy peak displays a sublinear power dependence and a noticeable energy blueshift, as highlighted in Figure 1b. Moreover, Figure 1c shows the temperature dependent PL spectra of the WS<sub>2</sub> monolayer, in which the lower energy PL peak presents an intensity reduction and an energy redshift under increasing temperature. Additionally, in Supporting Figure S1 it is possible to note that this lower energy peak vanishes at room temperature. A lower energy PL emission with sublinear power and temperature dependencies as described above is commonly related to defect-bound localized excitons ( $X_L$ ).<sup>28</sup> Nonetheless, this feature is reported in a variety of defects in TMDs, such as vacancy,<sup>29</sup> substitutional doping<sup>30,31</sup> and adsorbed impurities.<sup>29,32-36</sup> On the other

hand, the significant energy shift displayed for both power and temperature variation as well as the large spectral linewidth was previously related to the adsorption of oxygen and organic molecules due to an aging process in TMDs.<sup>32-36</sup>

In order to further characterize these samples, we employed XPS measurements (see Methods Section for experimental details). The valence state of each element present in the WS<sub>2</sub> monolayer was investigated using the high-resolution XPS spectra analysis. The analysis was used to validate the existence of a minor fraction of adsorbent defect sites within their structures, as done in Ref.<sup>36</sup> Figure 1d displays the spectrum of W 4d, which reveals the presence of two asymmetric responses associated with W 4d<sub>5/2</sub> and W 4d<sub>3/2</sub> orbitals.<sup>37</sup> Each one of these asymmetric orbital responses were fitted with two Voigt peaks. While the predominant fitted peaks (in blue) at 244.8 and 257.2 eV are related to the chemical state doublet of the W-S bond, the orange fitted peaks at 249.2 and 261.3 eV indicate the presence of a distinct chemical state doublet in a higher binding energy. Moreover, XPS high-resolution spectra of the aged WS<sub>2</sub> monolayer for the W 4f orbitals also exhibit an asymmetric response due to the presence of a defective chemical state doublet (see Supporting Figure S2). Similar XPS results were previously reported for an aged WS<sub>2</sub> monolayer and were related to a loss of sulfur atoms and a higher oxidation state for tungsten atoms as well as to the presence of non-identified adsorbed organic molecules.<sup>32,36</sup> Therefore, our XPS measurements give an indication that the defects responsible for the lower energy PL peak are similar to those found in Refs.<sup>32,36</sup>

In order to investigate the circular dichroism of the X<sub>L</sub> peak and its dependence with perpendicular external magnetic field, we performed circular polarization magneto-PL measurements at 4 K. The sample was excited by a linearly polarized laser beam, with an incident power of 100 μW and applying a perpendicular external magnetic field tunable from -9 to 9 T (in steps of 0.1 T), while its PL emission was detected for both right ( $\sigma^+$ ) and left ( $\sigma^-$ ) circular polarizations. Figures 2a,b exhibit the PL spectra for -9, 0 and 9 T for both  $\sigma^+$  and  $\sigma^-$  detection. An opposite energy shift with respect to the magnetic field for  $\sigma^+$  and  $\sigma^-$

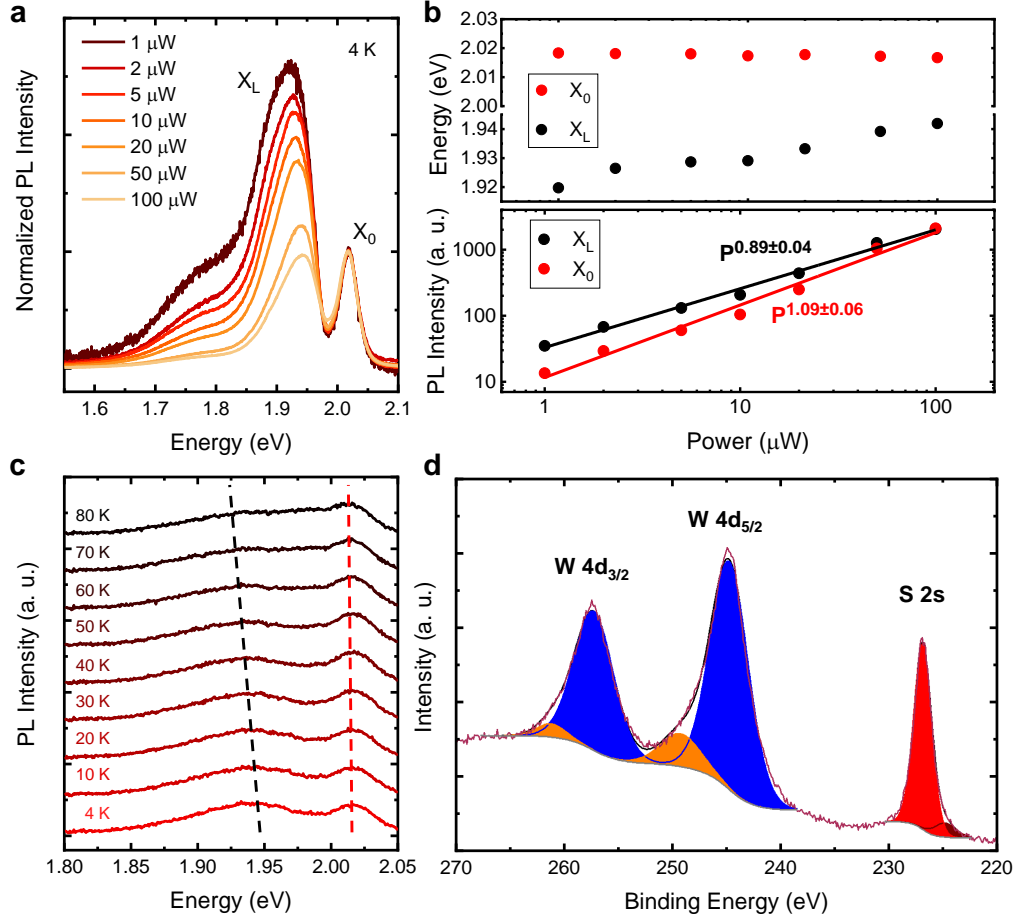


Figure 1: **a** Power dependent PL spectra at 4 K for an aged  $\text{WS}_2$  monolayer showing free exciton and defect-bound exciton peaks. PL spectra are normalized by the intensity of the free exciton peak. **b** PL energy (top graph) and intensity (bottom graph) dependencies on the incident power for both defect and exciton PL peaks. **c** Temperature dependent PL spectra for a  $100 \mu\text{W}$  incident power. All measurements were performed with a 532 nm laser. **d** XPS spectrum of W 4d and S 2s core-level peaks. The W 4d displays two W  $4d_{5/2}$  and W  $4d_{3/2}$  doublets associated to W of the main  $\text{WS}_2$  structure (blue fitted peaks) and to W at defect sites (orange fitted peaks).

emissions can be observed for both  $X_0$  and  $X_L$  peaks. A complete perspective of this shifting can be noted in the PL intensity 2D plots of Figures 2c,d, which contains all 181 PL spectra measured varying the external magnetic for both polarizations. This opposite energy shift occurs due to the Zeeman effect, that displaces each valley in opposite directions in energy as they present inverse spins. Besides, Figures 2a-d also shows the broadening of the  $X_L$  peak and its redshift with magnetic field. The magnetic field dependence of the valley Zeeman splitting  $\Delta E$  - denoted as the energy difference between  $\sigma^+$  and  $\sigma^-$  emission ( $E_{\sigma^+} - E_{\sigma^-}$ )

- is given by  $\Delta E = g\mu_B B$ , in which  $\mu_B = 0.05788$  meV/T is the Bohr magneton and  $g$  is the g-factor.<sup>5,6,9</sup> Thus, first we extracted the energy position of  $X_0$  and  $X_L$  peaks for all PL spectra, as shown in Figures 2e,f. From the energy values, we plotted the valley Zeeman splitting for  $X_0$  and  $X_L$  peaks and calculated their associated g-factors from the data linear fitting, as presented in Figure 2g,h. A g-factor of  $-(3.58 \pm 0.03)$  is obtained for the  $X_0$  peak, which is in agreement with previously reported values.<sup>4-7</sup> On the other hand, an enhanced g-factor of  $-(25.0 \pm 0.2)$  can be observed for the  $X_L$  peak, which corresponds to its noticeable energy shift shown in the magneto-PL spectra of Figures 2a-d. We performed similar measurements in another aged  $\text{WS}_2$  monolayer and we noticed this enhanced  $X_L$  g-factor for it as well, as displayed in Supporting Figure S3.

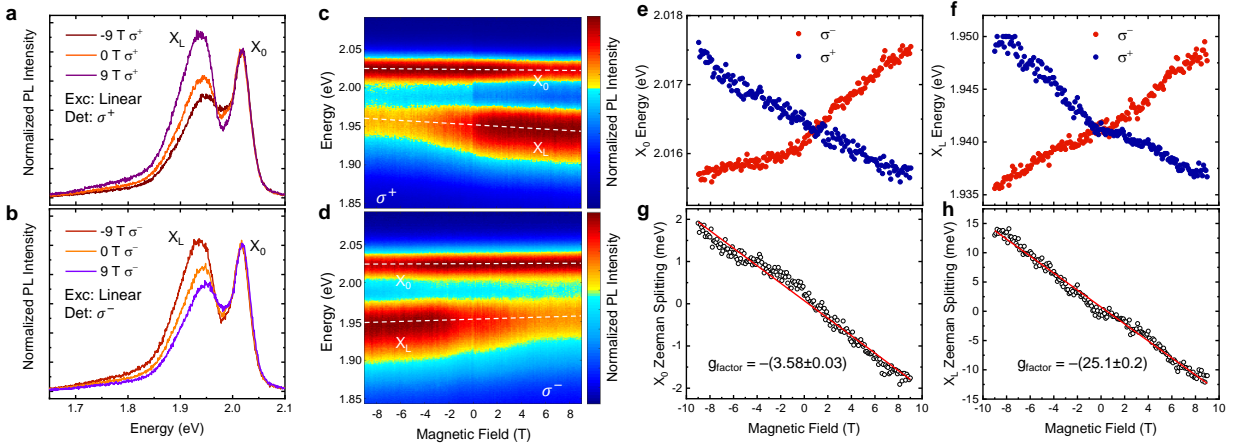


Figure 2: **a,b** PL spectra of an aged  $\text{WS}_2$  monolayer for a linearly polarized excitation and  $\sigma^+$  (**a**) and (**b**)  $\sigma^-$  detection with external magnetic fields of  $-9$ ,  $0$  and  $9$  T. **c,d** PL intensity 2D plots for linearly polarized excitation and  $\sigma^+$  (**c**) and (**d**)  $\sigma^-$  detection with external magnetic fields ranging from  $-9$  to  $9$  T. The spectra in (**a-d**) are normalized by the free exciton peak intensity to highlight the intensity and energy modifications in the defect-bound exciton peak. **e,f** Exciton (**e**) and defect-bound (**f**) PL peak energies with respect to the magnetic field and their respective valley Zeeman splitting showing g-factors of  $-(3.58 \pm 0.03)$  (**g**) and  $-(25.0 \pm 0.2)$  (**h**). All measurements were carried out at  $4$  K and with an incident power of  $100 \mu\text{W}$ .

To have a better understanding of the defect role in the optical properties of other aged TMDs, we investigated a 3-year aged CVD grown  $\text{WSe}_2$  monolayer by the same measurements carried out for the  $\text{WS}_2$  monolayer. Figure 3a shows the power dependent PL spectra at  $4$  K for the  $\text{WSe}_2$  monolayer normalized by the exciton peak intensity. Beyond the exciton

emission, it can also be observed a lower energy PL peak with a sublinear power dependence. Figures 3b,c show the power dependence of both exciton and defect PL peaks with respect to their energy and intensity, respectively. Similarly to the aged WS<sub>2</sub> monolayer, an energy blueshift and a sublinear intensity dependence under increasing power are noted for the defect-bound exciton peak in the WSe<sub>2</sub> sample. Moreover, temperature dependent PL measurements shown in Figure 3d reveals another similar behavior with respect to the WS<sub>2</sub> monolayer. As XPS measurements of this aged WSe<sub>2</sub> monolayer also shows the presence of an extra chemical bond (see Supporting Figure S2), it is suggestive that both WS<sub>2</sub> and WSe<sub>2</sub> lower energy PL peaks have the same defective source, since they were similarly grown and aged. Low temperature magneto-PL measurements with linear polarized excitation and circular polarized detection were also performed for the aged WSe<sub>2</sub> monolayer. Figures 3e,f shows the  $\sigma^+$  and  $\sigma^-$  detected PL spectra for all 181 measured external magnetic fields between  $-9$  and  $9$  T (with steps of  $0.1$  T), respectively. The individual PL spectra for  $-9$ ,  $0$  and  $9$  T are displayed in Supporting Figure S4. The energy of  $X_0$  and  $X_L$  peaks were extracted for all PL spectra and are presented in Figures 3g,h. Besides the well-known Zeeman shifting of the  $X_0$  peak, it is also noted a remarkable shift in the  $X_L$  PL peak for this aged WSe<sub>2</sub> monolayer. From its peak energy shift with magnetic field data it was calculated the valley Zeeman splitting for both exciton and defect-bound peaks, which are respectively shown in Figures 3i,j. A g-factor value of  $-(3.16 \pm 0.02)$  is retrieved for  $X_0$ , whereas  $X_L$  presenten a large g-factor of  $-(19.1 \pm 0.2)$ . Furthermore, Figures 3e,f also display the significant spectral broadening of the circular polarized  $X_L$  emission followed by an energy redshift with magnetic field.

As observed in Figures 2 and 3, beyond the large Zeeman shift of the  $X_L$  peak, this defect-bound exciton emission also presents a large circular polarized intensity dependence with magnetic field for both aged WS<sub>2</sub> and WSe<sub>2</sub> monolayers. To further investigate this dependence, we analyzed the degree of circular polarization (DCP) of the aged WSe<sub>2</sub> mono-

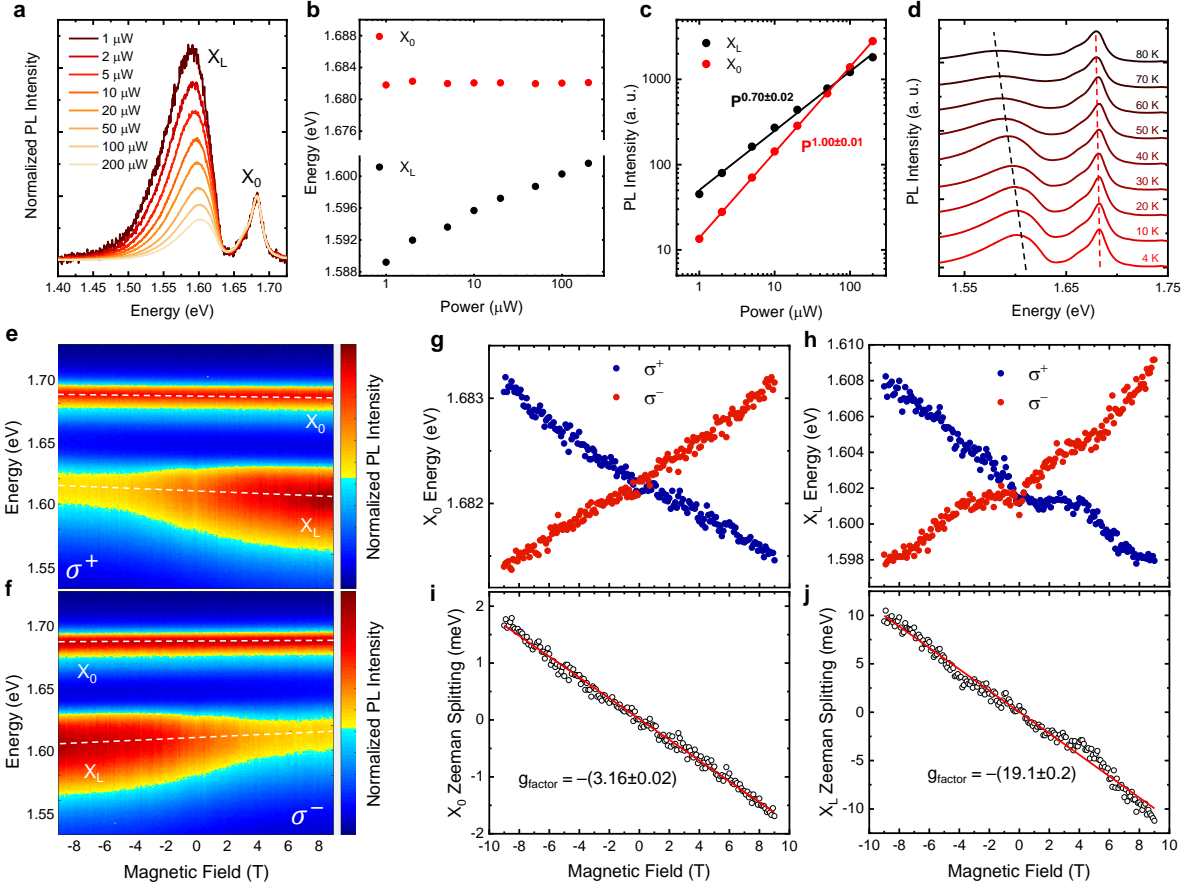


Figure 3: **a** Power dependent PL spectra at 4 K for aged WSe<sub>2</sub> monolayer showing free exciton and defect-bound exciton peaks. PL spectra are normalized by the intensity of the free exciton peak. PL energy (**b**) and intensity (**c**) dependencies with respect to the incident power for both defect and exciton PL peaks. **d** Temperature dependent PL spectra for 100  $\mu$ W incident power. **e, f** PL 2D plots for linear polarized excitation and  $\sigma^+$  (**e**) and  $\sigma^-$  (**f**) detection with external magnetic fields ranging from  $-9$  to  $9$  T. The spectra were normalized by the free exciton peak intensity to highlight the intensity and energy dependencies for the defect-bound exciton peak. Exciton (**g**) and defect (**h**) PL peak energies with respect to the magnetic field and their respective valley Zeeman splitting showing  $g$ -factors of  $-(3.16 \pm 0.02)$  (**i**) and  $-(19.1 \pm 0.2)$  (**j**). All magneto-PL measurements were carried out at 4 K and with an incident power of 100  $\mu$ W.

layer, given by:

$$\text{DCP}(\%) = 100 \frac{I_{\sigma^+} - I_{\sigma^-}}{I_{\sigma^+} + I_{\sigma^-}},$$

in which  $I_{\sigma^+}$  and  $I_{\sigma^-}$  are the PL intensities for both  $\sigma^+$  and  $\sigma^-$  polarizations, respectively. Figure 4a shows the DCP of the aged WSe<sub>2</sub> monolayer for  $-9$ ,  $0$  and  $9$  T. They were plotted by subtracting the  $\sigma^+$  PL spectrum by the  $\sigma^-$  PL spectrum and dividing the result by

the sum of  $\sigma^+$  and  $\sigma^-$  PL spectra. A negligible DCP can be observed for the whole PL spectral range at 0 T, that is a consequence of the similar PL spectra for both  $\sigma^+$  and  $\sigma^-$  detection at 0 T. This absence of DCP is related to the symmetric band structure with anti-symmetric spin moments at 0 T between K and  $-K$  valleys. On the other hand, we can observe a significant variation of the DCP for  $-9$  and  $9$  T with respect to the emission energy. While there is a DCP of  $\sim 7.5\%$  in the  $X_0$  spectral range, the  $X_L$  peak energy shows an increased DCP of  $\sim 40\%$ , more than 5 times greater compared to  $X_0$ . In addition, from the PL spectra fitting we extracted the intensities of  $X_0$  and  $X_L$  for all measured external magnetic fields, as displayed in Figures 4b,c. The  $\sigma^+$  and  $\sigma^-$  PL intensities of the free exciton are maximum close to 0 T and decrease for both positive and negative magnetic fields. Conversely, the defect-bound exciton PL intensity dependence on the magnetic field is approximately linear, with a positive (negative) slope for  $\sigma^+$  ( $\sigma^-$ ) emission. While  $\sigma^+$  and  $\sigma^-$  polarized  $X_L$  emissions have similar intensities at  $B = 0$ , for  $B = 9$  T the  $X_L$   $\sigma^+$  polarized intensity is 2.5 times greater than the  $X_L$   $\sigma^-$  polarized intensity (and the opposite is valid for  $B = -9$  T), revealing a significant magnetic field induced spin polarization of the mid gap states. In addition, the aged  $\text{WS}_2$  monolayer also shows a noticeable DCP for the  $X_L$  peak, as shown in Supporting Figure S5. Therefore, we can note a correspondence of the magnetic field dependence between the  $X_L$  peak energy shifting, spectral broadening and spin polarization. These relationships will be discussed below to explain the observed giant g-factor of the defect-bound exciton peak.

The Zeeman shift in TMDs are due to the orbital, spin and valley magnetic moments of the valence and the conduction bands of the material. The reported g-factors of the  $X_0$  state related to the valley Zeeman splitting between K and  $-K$  valleys is around  $-4\mu_B$ .<sup>4-7</sup> TMD monolayers present the same spin magnetic moments between the valence and conduction bands, not presenting thus any influence in their Zeeman splitting.<sup>9</sup> Moreover, their valley magnetic moment are associated with the Berry curvatures of their bands.<sup>9</sup> Hence, in a first approximation in which the electron and hole effective masses are equal, the valence

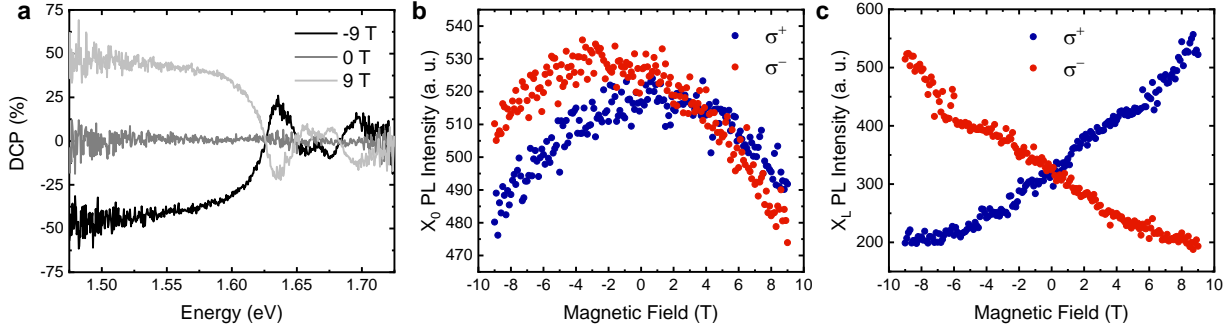


Figure 4: **a** Degree of circular polarization of an aged WSe<sub>2</sub> monolayer for  $-9$ ,  $0$  and  $9$  T between  $\sigma^+$  and  $\sigma^-$  PL spectra. Free exciton (**b**) and defect-bound exciton (**c**) PL intensities with respect to the magnetic field.

and conduction bands Berry curvatures are also the same.<sup>9</sup> Therefore, the valley Zeeman splitting of TMD monolayers is mainly governed by the distinct orbital magnetic moments of their conduction and valence bands. While their  $d_{z^2}$  conduction band orbital has a zero magnetic moment, their hybridized  $d_{x^2-y^2} \pm id_{xy}$  valence band orbitals have orbital magnetic moments of  $\mu_l = \pm 2\mu_B$ , related to the K and  $-K$  valleys, respectively.<sup>1</sup> Hence, in this approach the total valley Zeeman splitting between K and  $-K$  valleys associated with the X<sub>0</sub> state is  $-4\mu_B$ . As defect-bound exciton PL peaks are related to the optical transition from defective mid gap states to the valence band, a distinct valley Zeeman splitting is expected.<sup>23</sup> Although spin magnetic moments remain the same, orbital and valley magnetic moments can be deeply modified, since the mid gap states can present distinct hybridized orbitals and Berry curvatures with respect to the valence band. For instance, a  $-6.2$  g-factor associated with vacancy defective levels in MoS<sub>2</sub> monolayers was previously explained by their distinct magnetic moments.<sup>23</sup> However, such argument cannot fully explain our observation of the giant g-factor values for the aged monolayers, and therefore require a further explanation.

Comparing the power dependent PL spectra (Figures 1a and 3a) with the magnetic field dependent PL spectra (Figures 2a-d and 3e,f) it is clearly noted a similar dependence of the X<sub>L</sub> peak with pumping power and applied magnetic field. As previously reported, the adsorbent defects can induce the emergence of an ensemble of distinct mid gap states,<sup>36</sup> leading to the observed broad PL peaks.<sup>29,35,36</sup> Therefore, by varying the incident power

there are modifications in the charge carrier occupation of these mid gap states, resulting in a significant peak energy shift. Figure 5 schematically represents this light emission power dependence by showing the band structure of a direct gap semiconductor with two mid gap states at low and high excitation power regimes. For low excitation powers, the lower energy defective level is more occupied due to the charge carrier relaxation, leading to a lower energy defect-bound exciton emission. For high incident powers, the electronic occupation of the lower energy mid gap state saturates, resulting in a larger occupation of the higher energy mid gap state and a blueshift of the broad defect-bound exciton emission. Similarly, the defect-bound exciton magneto-optical responses might be related to a magnetic field dependent occupation of the mid gap states.

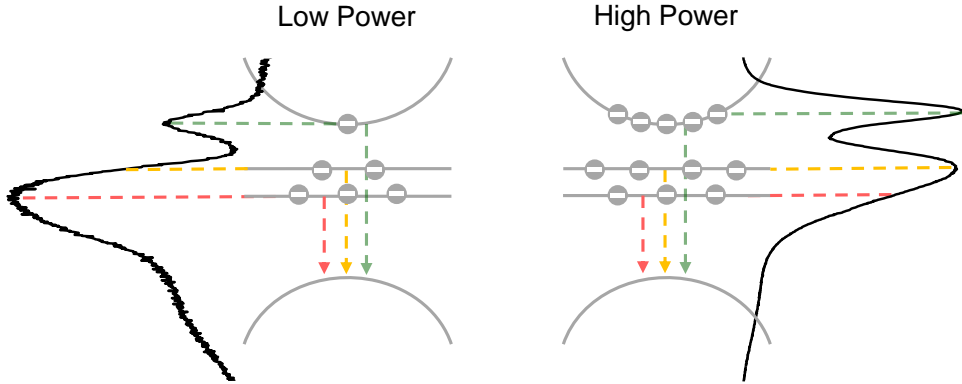


Figure 5: Illustrative representation of the radiative recombination from the conduction band and mid gap states for a low and high incident power regime in a direct gap semiconductor. The PL spectra of the aged  $\text{WS}_2$  monolayer with excitation powers of 1 and  $100 \mu\text{W}$  are displayed besides each band structure diagram to associate their energy shift with the electronic occupation of the mid gap states.

Figure 6a summarizes the dependence of the aged  $\text{WS}_2$  and  $\text{WSe}_2$  monolayers optical responses on the external magnetic field, in which the  $\sigma^+$  polarized light emission at the K valley is represented for negative, zero and positive magnetic fields. Experimentally we have found that for positive magnetic fields, the radiative recombinations from the mid gap states — related to the  $X_L$  PL peak — exhibit an intensity enhancement, an energy redshift and a spectral broadening compared to the emission without an external magnetic

field. Conversely, for negative magnetic fields there is an intensity reduction, an energy blueshift and a spectral narrowing of the  $X_L$  peak emission. The opposite is valid for the  $\sigma^-$  polarized light emission at the  $-K$  valley. Considering this scenario, we next propose a spin-flip mechanism to explain these experimental observations, as represented in Figure 6b.

Distinct relaxation pathways are reported in the electronic dynamics of TMD monolayers. For instance, intervalley and intravalley scattering of excited carriers can happen due to electron-phonon and spin-orbit interactions, respectively.<sup>38,39</sup> The intravalley scattering is associated with a spin-flip of the carrier state, and can also be induced by an external magnetic field.<sup>38,40</sup> For mid gap states, similar relaxations can occur as well. As our reported aging defects are non-magnetic, it is expected smaller spin splittings of their electronic levels, as shown in Figure 6a. Therefore, as the spin splitted defective mid gap states are closer in energy, it is reasonable to expect a greater probability of electronic relaxation among them. In addition, the electronic recombination of electrons in these trapping states is notably slower than of free excitons,<sup>41,42</sup> which also favors the relaxation processes in the mid gap levels. Therefore, we presume that the external magnetic fields induce significant spin-flip transitions between the spin splitted mid gap states. As shown in Figure 6b, while there is no relevant spin-flip transition in the absence of an external magnetic field, positive (negative) magnetic fields cause spin-flip transitions from spin-down (-up) to spin-up (-down) states, leading to a strong spin polarization in the mid gap states. Hence, for positive (negative) magnetic fields there will be a dominant population of spin-up (-down) states, which is in agreement with the enhanced (quenched), redshifted (blueshifted) and broadened (narrowed)  $\sigma^+$  polarized light emission observed in the experimental results and depicted in Figure 6a. It is important to comment that the defective levels are also shifted by the external magnetic fields, as shown in 6a. Therefore, it is also possible that the Zeeman shift causes accidental degeneracies between spin-up and spin-down mid gap states, contributing even more to the spin-flip transitions.

In summary, we studied aged  $WS_2$  and  $WSe_2$  monolayers by power dependent PL, tem-

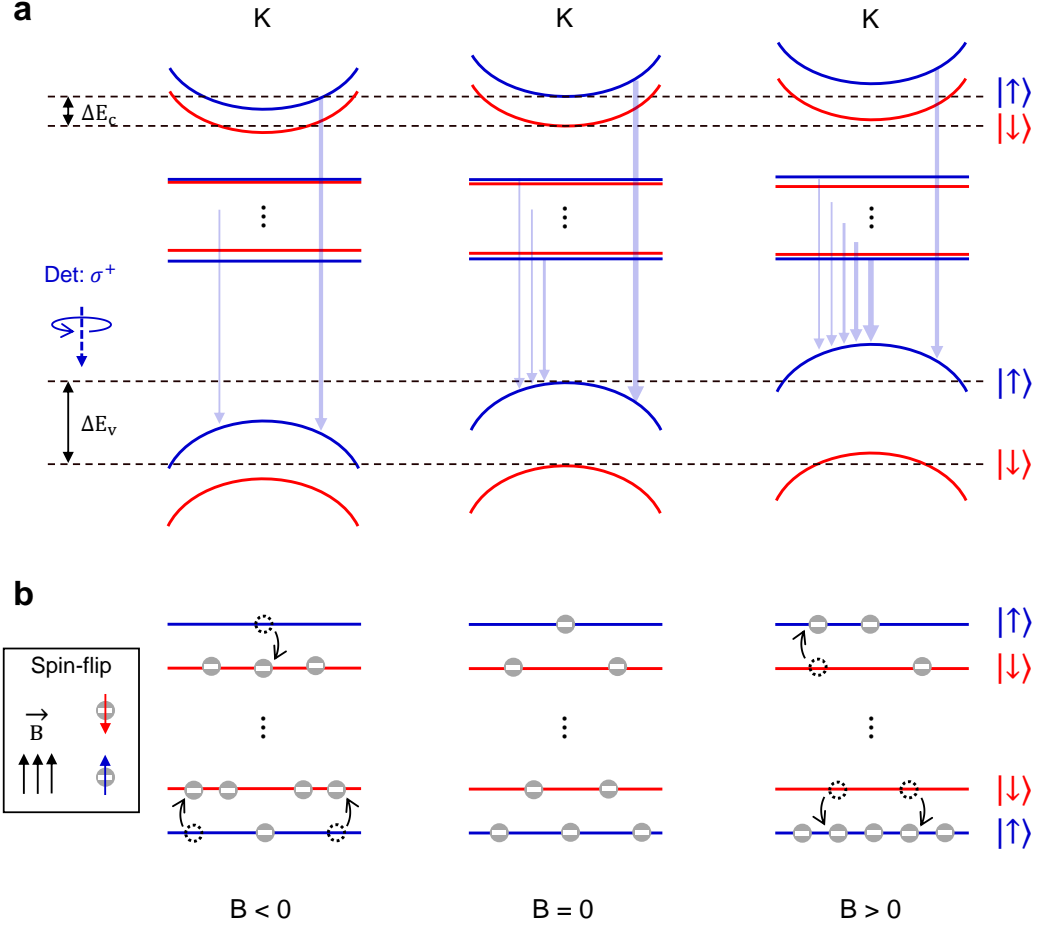


Figure 6: **a** Band structure representation of an aged  $\text{WS}_2$  or  $\text{WSe}_2$  monolayer for negative, zero and positive magnetic fields, showing the conduction and valence bands Zeeman shifting and the multiple spin splitted mid gap states. The blue arrows represents the possible spin allowed optical transitions for  $\sigma_+$  detection. The number and thickness of the arrows corresponds to the experimentally observed PL broadening and intensity respectively. **b** Spin-flip relaxation in the mid gap states induced by the external magnetic fields. The spin polarized population of these defective levels lead to their magnetic dependent light emission shown in **(a)**.

perature dependent PL and low temperature circularly polarized magneto-PL measurements. The power and temperature dependent PL spectra showed a lower energy peak related to a defect-bound exciton. XPS measurements were carried out and related this lower energy PL peak to the presence of an extra chemical bond to the W atom that might be associated with the adsorption of oxygen and organic molecules in the material structure. Finally, low temperature circularly polarized PL measurements with a varying external magnetic field were performed to study the Zeeman effect in the defect-bound exciton. A significant energy

shift of the defective emission corresponding to an intensity enhancement and a spectral broadening was observed for both aged monolayers under magnetic field variation. From their Zeeman splitting we extracted g-factor values of  $-(25.0 \pm 0.2)$  and  $-(19.1 \pm 0.2)$  for the defect-bound exciton emission in  $\text{WS}_2$  and  $\text{WSe}_2$  monolayers, respectively. In addition, the aged samples presented a notable spin polarization of the mid gap states induced by the external magnetic field. This spin polarized population lead to a magnetic field dependent distribution of charge carriers in the multiple defective levels, which contributes to the giant effective g-factor of the defect-bound exciton. A spin-flip transition mechanism was proposed to explain the observed spin polarization. Our work highlights how adsorbed defects related to an aging process can potentialize the Zeeman splitting and carriers spin polarization in TMD monolayers for spintronics and valleytronics applications.

## Methods

### Sample Preparation

The monolayer  $\text{WS}_2$  and  $\text{WSe}_2$  samples were prepared using a liquid-phase precursor-assisted deposition method that we developed earlier.<sup>43</sup> In brief, 50 mg of ammonium metatungstate hydrate  $[(\text{NH}_4)_6\text{H}_2\text{W}_{12}\text{O}_{40} \cdot x\text{H}_2\text{O}]$  and 200 mg of sodium cholate hydrate  $(\text{C}_{24}\text{H}_{39}\text{NaO}_5 \cdot x\text{H}_2\text{O})$  powders were first dissolved in 10 ml of deionized (DI) water to form a precursor solution. The solution was then spin-coated on clean  $\text{SiO}_2/\text{Si}$  substrates, which were placed into a quartz tube together with 300 mg of sulfur (S) or 120 mg of selenium (Se) powders upstream. The quartz tube was placed in a two-zone furnace and heated at 800 °C for 15 min with argon (Ar) streaming (for the  $\text{WSe}_2$  synthesis, an argon/hydrogen (Ar/ $\text{H}_2$ ) mixture was applied instead). After the reaction, the whole setup was cooled down to room temperature naturally with Ar protection.

## Spectroscopy Measurements

The temperature, power and magneto dependent PL spectroscopy measurements were carried out in a confocal microscope coupled to a magneto-cryostat (Attocube — Attodry 1000). We performed these measurements by varying the temperature from 4 to 80 K and the applied magnetic field from  $-9$  to  $9$  T, in which the magnetic field direction was perpendicular to the samples plane. The samples were excited by a linear polarized laser beam with excitations wavelengths of 532 nm (Cobolt — 08 series) and 660 nm (Toptica — iBeam) for the aged WS<sub>2</sub> and WSe<sub>2</sub> monolayers, respectively. The  $\sigma^+$  and  $\sigma^-$  polarized PL emissions were filtered by a linear polarizer and a quarter-wave plate and detected in a spectrometer equipped with a sensitive CCD camera (Andor — Shamrock-Idus).

## X-ray Photoelectron Spectroscopy Measurements

The measurements were conducted using a monochromatic Al K $\alpha$  X-ray source and a Phoibos 150 electron analyzer from SPECS. The high-resolution spectra acquisition was carried out using passage energy of 30 eV with an energy step of 0.1 eV. All spectra were calibrated with respect to the energy reference of the C 1s peak, derived from adventitious carbon, positioned at 284.6 eV. The experimental data were adjusted through a combination of Voigt curve components employing a Shirley background. During the curve fitting of the high-resolution W 4f and W 4d spectra, the area ratio between the doublet peaks was constrained, taking into account the theoretical electronic distribution of each orbital at the respective energy levels.

## Acknowledgement

F.B.S. and L.M.M. acknowledges financial support from CNPq, CAPES, FAPEMIG (APQ-01171-21), FINEP, Brazilian Institute of Science and Technology (INCT) in Carbon Nanomaterials and Rede Mineira de Materiais 2D (FAPEMIG). A.M., V.A.O. and M.D.T. ac-

knowledges financial support from FAPESP (2015/13771-0 and 2022/10340-2). M.T., M.L. and D.Z. also thank AFOSR for financial support (FA9550-23-1-0447).

## References

- (1) Xiao, D.; Liu, G.-B.; Feng, W.; Xu, X.; Yao, W. Coupled Spin and Valley Physics in Monolayers of MoS<sub>2</sub> and Other Group-VI Dichalcogenides. *Physical Review Letters* **2012**, *108*, 196802.
- (2) Mak, K. F.; He, K.; Shan, J.; Heinz, T. F. Control of valley polarization in monolayer MoS<sub>2</sub> by optical helicity. *Nature Nanotechnology* **2012**, *7*, 494–498.
- (3) Cao, T.; Wang, G.; Han, W.; Ye, H.; Zhu, C.; Shi, J.; Niu, Q.; Tan, P.; Wang, E.; Liu, B.; Feng, J. Valley-selective circular dichroism of monolayer molybdenum disulfide. *Nature Communications* **2012**, *3*, 887.
- (4) Li, Y.; Ludwig, J.; Low, T.; Chernikov, A.; Cui, X.; Arefe, G.; Kim, Y. D.; van der Zande, A. M.; Rigosi, A.; Hill, H. M.; Kim, S. H.; Hone, J.; Li, Z.; Smirnov, D.; Heinz, T. F. Valley Splitting and Polarization by the Zeeman Effect in Monolayer MoSe<sub>2</sub>. *Physical Review Letters* **2014**, *113*, 266804.
- (5) Aivazian, G.; Gong, Z.; Jones, A. M.; Chu, R.-L.; Yan, J.; Mandrus, D. G.; Zhang, C.; Cobden, D.; Yao, W.; Xu, X. Magnetic control of valley pseudospin in monolayer WSe<sub>2</sub>. *Nature Physics* **2015**, *11*, 148–152.
- (6) Srivastava, A.; Sidler, M.; Allain, A. V.; Lembke, D. S.; Kis, A.; Imamoglu, A. Valley Zeeman effect in elementary optical excitations of monolayer WSe<sub>2</sub>. *Nature Physics* **2015**, *11*, 141–147.
- (7) MacNeill, D.; Heikes, C.; Mak, K. F.; Anderson, Z.; Kormányos, A.; Zólyomi, V.;

- Park, J.; Ralph, D. C. Breaking of Valley Degeneracy by Magnetic Field in Monolayer MoSe<sub>2</sub>. *Physical Review Letters* **2015**, *114*, 37401.
- (8) Ahn, E. C. 2D materials for spintronic devices. *npj 2D Materials and Applications* **2020**, *4*, 17.
- (9) Stier, A. V.; McCreary, K. M.; Jonker, B. T.; Kono, J.; Crooker, S. A. Exciton diamagnetic shifts and valley Zeeman effects in monolayer WS<sub>2</sub> and MoS<sub>2</sub> to 65 Tesla. *Nature Communications* **2016**, *7*, 10643.
- (10) Plechinger, G.; Nagler, P.; Arora, A.; Granados del Águila, A.; Ballottin, M. V.; Frank, T.; Steinleitner, P.; Gmitra, M.; Fabian, J.; Christianen, P. C. M.; Bratschkitsch, R.; Schüller, C.; Korn, T. Excitonic Valley Effects in Monolayer WS<sub>2</sub> under High Magnetic Fields. *Nano Letters* **2016**, *16*, 7899–7904.
- (11) Lyons, T. P.; Dufferwiel, S.; Brooks, M.; Withers, F.; Taniguchi, T.; Watanabe, K.; Novoselov, K. S.; Burkard, G.; Tartakovskii, A. I. The valley Zeeman effect in inter- and intra-valley trions in monolayer WSe<sub>2</sub>. *Nature Communications* **2019**, *10*, 2330.
- (12) Nagler, P.; Ballottin, M. V.; Mitioglu, A. A.; Durnev, M. V.; Taniguchi, T.; Watanabe, K.; Chernikov, A.; Schüller, C.; Glazov, M. M.; Christianen, P. C.; Korn, T. Zeeman Splitting and Inverted Polarization of Biexciton Emission in Monolayer WS<sub>2</sub>. *Physical Review Letters* **2018**, *121*, 57402.
- (13) Barbone, M. et al. Charge-tuneable biexciton complexes in monolayer WSe<sub>2</sub>. *Nature Communications* **2018**, *9*, 3721.
- (14) Nagler, P.; Ballottin, M. V.; Mitioglu, A. A.; Mooshammer, F.; Paradiso, N.; Strunk, C.; Huber, R.; Chernikov, A.; Christianen, P. C. M.; Schüller, C.; Korn, T. Giant magnetic splitting inducing near-unity valley polarization in van der Waals heterostructures. *Nature Communications* **2017**, *8*, 1551.

- (15) Wang, T.; Miao, S.; Li, Z.; Meng, Y.; Lu, Z.; Lian, Z.; Blei, M.; Taniguchi, T.; Watanabe, K.; Tongay, S.; Smirnov, D.; Shi, S.-F. Giant Valley-Zeeman Splitting from Spin-Singlet and Spin-Triplet Interlayer Excitons in WSe<sub>2</sub>/MoSe<sub>2</sub> Heterostructure. *Nano Letters* **2020**, *20*, 694–700.
- (16) Holler, J.; Selig, M.; Kempf, M.; Zipfel, J.; Nagler, P.; Katzer, M.; Katsch, F.; Ballottin, M. V.; Mitioğlu, A. A.; Chernikov, A.; Christianen, P. C. M.; Schüller, C.; Knorr, A.; Korn, T. Interlayer exciton valley polarization dynamics in large magnetic fields. *Physical Review B* **2022**, *105*, 85303.
- (17) Gobato, Y. G.; de Brito, C. S.; Chaves, A.; Prosnikov, M. A.; Woźniak, T.; Guo, S.; Barcelos, I. D.; Milošević, M. V.; Withers, F.; Christianen, P. C. M. Distinctive g-Factor of Moiré-Confined Excitons in van der Waals Heterostructures. *Nano Letters* **2022**, *22*, 8641–8646.
- (18) He, Y.-M.; Clark, G.; Schaibley, J. R.; He, Y.; Chen, M.-C.; Wei, Y.-J.; Ding, X.; Zhang, Q.; Yao, W.; Xu, X.; Lu, C.-Y.; Pan, J.-W. Single quantum emitters in monolayer semiconductors. *Nature Nanotechnology* **2015**, *10*, 497–502.
- (19) Koperski, M.; Nogajewski, K.; Arora, A.; Cherkez, V.; Mallet, P.; Veuillen, J.-Y.; Marcus, J.; Kossacki, P.; Potemski, M. Single photon emitters in exfoliated WSe<sub>2</sub> structures. *Nature Nanotechnology* **2015**, *10*, 503–506.
- (20) Srivastava, A.; Sidler, M.; Allain, A. V.; Lembke, D. S.; Kis, A.; Imamoglu, A. Optically active quantum dots in monolayer WSe<sub>2</sub>. *Nature Nanotechnology* **2015**, *10*, 491–496.
- (21) Chakraborty, C.; Kinnischtzke, L.; Goodfellow, K. M.; Beams, R.; Vamivakas, A. N. Voltage-controlled quantum light from an atomically thin semiconductor. *Nature Nanotechnology* **2015**, *10*, 507–511.
- (22) Kuhnert, J.; Rahimi-Iman, A.; Heimbrodt, W. Magneto photoluminescence measure-

- ments of tungsten disulphide monolayers. *Journal of Physics: Condensed Matter* **2017**, *29*, 08LT02.
- (23) Wang, Y. et al. Spin-Valley Locking Effect in Defect States of Monolayer MoS<sub>2</sub>. *Nano Letters* **2020**, *20*, 2129–2136.
- (24) Dang, J.; Sun, S.; Xie, X.; Yu, Y.; Peng, K.; Qian, C.; Wu, S.; Song, F.; Yang, J.; Xiao, S.; Yang, L.; Wang, Y.; Rafiq, M. A.; Wang, C.; Xu, X. Identifying defect-related quantum emitters in monolayer WSe<sub>2</sub>. *npj 2D Materials and Applications* **2020**, *4*, 2.
- (25) Li, Q. et al. Enhanced Valley Zeeman Splitting in Fe-Doped Monolayer MoS<sub>2</sub>. *ACS Nano* **2020**, *14*, 4636–4645.
- (26) Zhou, J. et al. Synthesis of Co-Doped MoS<sub>2</sub> Monolayers with Enhanced Valley Splitting. *Advanced Materials* **2020**, *32*, 1906536.
- (27) Liu, H.; Fu, D.; Li, X.; Han, J.; Chen, X.; Wu, X.; Sun, B.; Tang, W.; Ke, C.; Wu, Y.; Wu, Z.; Kang, J. Enhanced Valley Splitting in Monolayer WSe<sub>2</sub> by Phase Engineering. *ACS Nano* **2021**, *15*, 8244–8251.
- (28) Tongay, S.; Suh, J.; Ataca, C.; Fan, W.; Luce, A.; Kang, J. S.; Liu, J.; Ko, C.; Raghunathan, R.; Zhou, J.; Ogletree, F.; Li, J.; Grossman, J. C.; Wu, J. Defects activated photoluminescence in two-dimensional semiconductors: interplay between bound, charged and free excitons. *Scientific Reports* **2013**, *3*, 2657.
- (29) Mitterreiter, E. et al. The role of chalcogen vacancies for atomic defect emission in MoS<sub>2</sub>. *Nature Communications* **2021**, *12*, 3822.
- (30) Loh, L.; Zhang, Z.; Bosman, M.; Eda, G. Substitutional doping in 2D transition metal dichalcogenides. *Nano Research* **2021**, *14*, 1668–1681.
- (31) Sousa, F. B.; Zheng, B.; Liu, M.; Resende, G. C.; Zhou, D.; Pimenta, M. A.; Terrones, M.; Crespi, V. H.; Malard, L. M. Effects of Vanadium Doping on the Optical Re-

- sponse and Electronic Structure of WS<sub>2</sub> Monolayers. *arXiv preprint arXiv:2401.09402* **2024**.
- (32) Gao, J.; Li, B.; Tan, J.; Chow, P.; Lu, T.-M.; Koratkar, N. Aging of Transition Metal Dichalcogenide Monolayers. *ACS Nano* **2016**, *10*, 2628–2635.
- (33) Lin, Z.; Carvalho, B. R.; Kahn, E.; Lv, R.; Rao, R.; Terrones, H.; Pimenta, M. A.; Terrones, M. Defect engineering of two-dimensional transition metal dichalcogenides. *2D Materials* **2016**, *3*, 22002.
- (34) He, Z.; Wang, X.; Xu, W.; Zhou, Y.; Sheng, Y.; Rong, Y.; Smith, J. M.; Warner, J. H. Revealing Defect-State Photoluminescence in Monolayer WS<sub>2</sub> by Cryogenic Laser Processing. *ACS Nano* **2016**, *10*, 5847–5855.
- (35) Krustok, J.; Kaupmees, R.; Jaaniso, R.; Kiisk, V.; Sildos, I.; Li, B.; Gong, Y. Local strain-induced band gap fluctuations and exciton localization in aged WS<sub>2</sub> monolayers. *AIP Advances* **2017**, *7*, 65005.
- (36) Xu, X.; Li, L.; Yang, M.; Guo, Q.; Wang, Y.; Li, X.; Zhuang, X.; Liang, B. Localized state effect and exciton dynamics for monolayer WS<sub>2</sub>. *Optics Express* **2021**, *29*, 5856–5866.
- (37) Romanov, R. I.; Kozodaev, M. G.; Chernikova, A. G.; Zabrosaev, I. V.; Chouprik, A. A.; Zarubin, S. S.; Novikov, S. M.; Volkov, V. S.; Markeev, A. M. Thickness-Dependent Structural and Electrical Properties of WS<sub>2</sub> Nanosheets Obtained via the ALD-Grown WO<sub>3</sub> Sulfurization Technique as a Channel Material for Field-Effect Transistors. *ACS Omega* **2021**, *6*, 34429–34437.
- (38) Jiang, Y.; Chen, S.; Zheng, W.; Zheng, B.; Pan, A. Interlayer exciton formation, relaxation, and transport in TMD van der Waals heterostructures. *Light: Science & Applications* **2021**, *10*, 72.

- (39) Robert, C. et al. Spin/valley pumping of resident electrons in WSe<sub>2</sub> and WS<sub>2</sub> monolayers. *Nature Communications* **2021**, *12*, 5455.
- (40) Slobodeniuk, A. O.; Basko, D. M. Spin–flip processes and radiative decay of dark intravalley excitons in transition metal dichalcogenide monolayers. *2D Materials* **2016**, *3*, 35009.
- (41) Wang, G.; Bouet, L.; Lagarde, D.; Vidal, M.; Balocchi, A.; Amand, T.; Marie, X.; Urbaszek, B. Valley dynamics probed through charged and neutral exciton emission in monolayer WSe<sub>2</sub>. *Physical Review B* **2014**, *90*, 75413.
- (42) Lagarde, D.; Bouet, L.; Marie, X.; Zhu, C. R.; Liu, B. L.; Amand, T.; Tan, P. H.; Urbaszek, B. Carrier and Polarization Dynamics in Monolayer MoS<sub>2</sub>. *Physical Review Letters* **2014**, *112*, 47401.
- (43) Zhang, T.; Fujisawa, K.; Zhang, F.; Liu, M.; Lucking, M. C.; Gontijo, R. N.; Lei, Y.; Liu, H.; Crust, K.; Granzier-Nakajima, T.; Terrones, H.; Elías, A. L.; Terrones, M. Universal In Situ Substitutional Doping of Transition Metal Dichalcogenides by Liquid-Phase Precursor-Assisted Synthesis. *ACS Nano* **2020**, *14*, 4326–4335.

**This Supporting Information includes:**

- Figure S1. Room temperature PL spectra for the aged WS<sub>2</sub> monolayer.
- Figure S2. XPS experiments for aged WS<sub>2</sub> and WSe<sub>2</sub> monolayers.
- Figure S3. Free exciton and defect-bound exciton Zeeman splittings for the aged WS<sub>2</sub> monolayer.
- Figure S4. Magneto-PL spectra for the aged WSe<sub>2</sub> monolayer.
- Figure S5. Degree of circular polarization for the aged WS<sub>2</sub> monolayer.

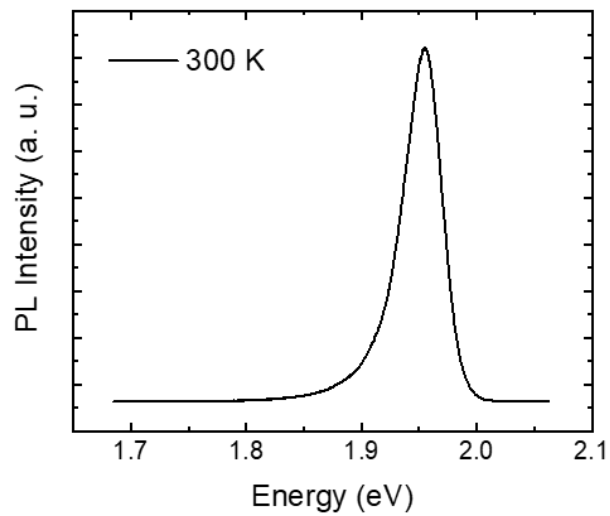


Figure S1: Room temperature PL spectra of the aged WS<sub>2</sub> monolayer showing no defect-bound exciton peak.

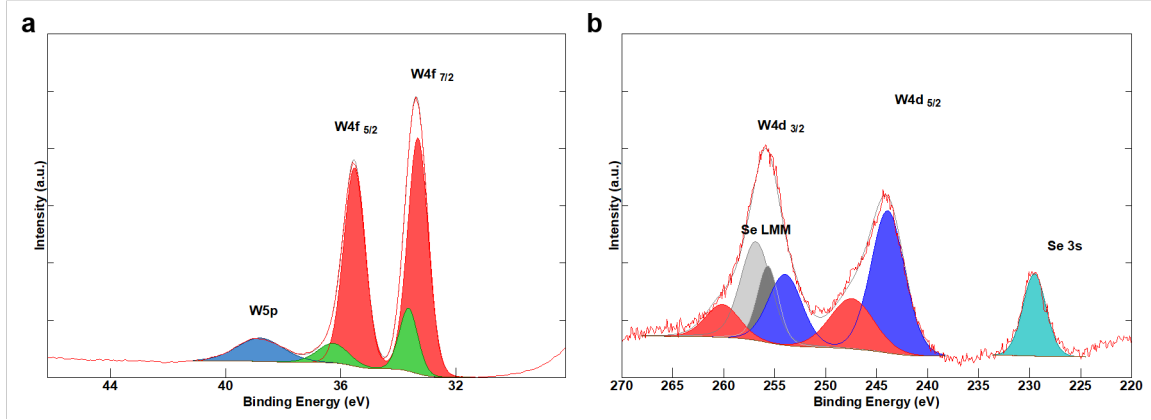


Figure S2: **a** XPS spectrum of W 4f and W 5p core-level peaks for an aged WS<sub>2</sub> monolayer. The W 4f displays two W 4f<sub>7/2</sub> and W 4f<sub>5/2</sub> doublets associated to W of the main WS<sub>2</sub> structure (red fitted peaks) and to W at defect sites (green fitted peaks). **b** XPS spectrum of W 4d and Se 2s core-level peaks for an aged WSe<sub>2</sub> monolayer. The W 4d display two W 4d<sub>5/2</sub> and W 4d<sub>3/2</sub> doublets associated to W of the main WSe<sub>2</sub> structure (blue fitted peaks) and to W at defect sites (red fitted peaks).

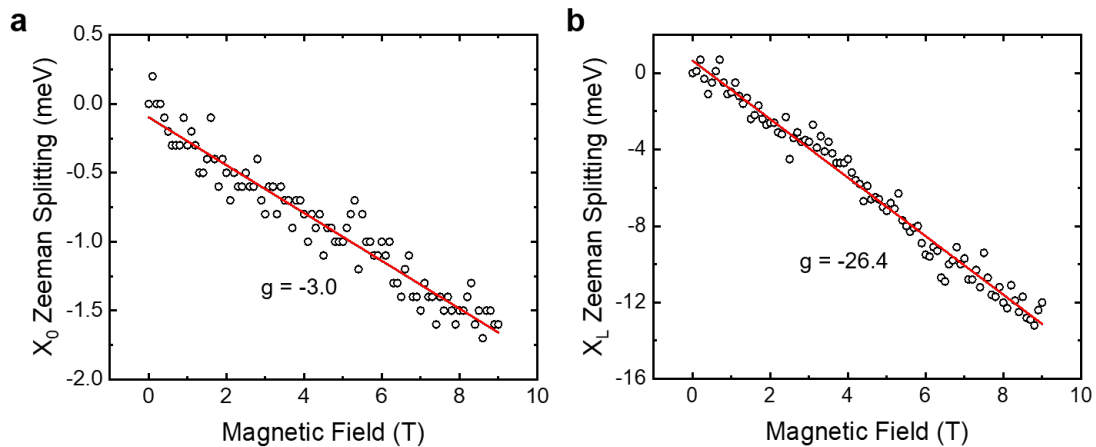


Figure S3: **a,b** Zeeman splittings related to exciton (**a**) and defect-bound exciton (**b**) transitions for an aged WS<sub>2</sub> monolayer measured with an incident power of 100  $\mu$ W. These measurements were performed in a different flake from that presented in Figure 2, confirming the great g-factor associated with the defective PL peak.

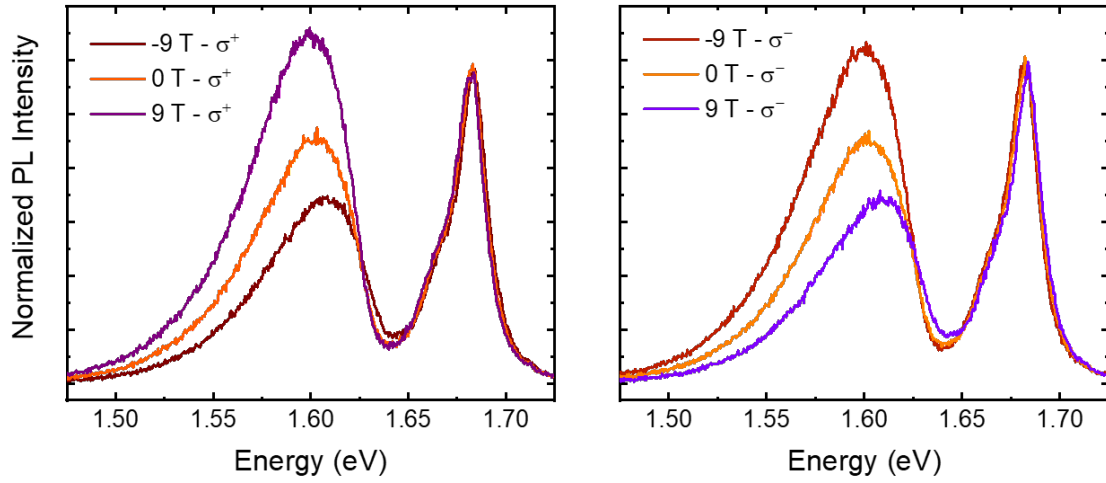


Figure S4: **a,b** PL spectra of an aged WS<sub>2</sub> monolayer for a linearly polarized excitation and  $\sigma^+$  (**a**) and  $\sigma^-$  (**b**) detections with external magnetic fields of  $-9$ ,  $0$  and  $9$  T. The spectra are normalized by the free exciton peak intensity.

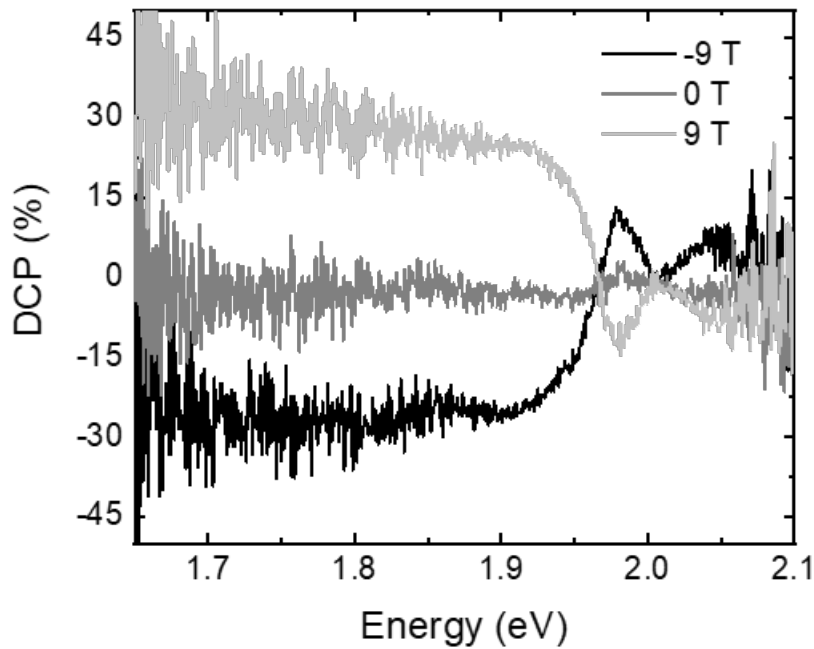


Figure S5: Degree of circular polarization of an aged WS<sub>2</sub> monolayer for  $-9$ ,  $0$  and  $9$  T between the  $\sigma^+$  and  $\sigma^-$  PL spectra shown in Figure 2.